WILEY-VCH

RESEARCH ARTICLE

Nordihydroguaiaretic Acid (NDGA) Inhibits CsgA Polymerization, Bacterial Amyloid Biogenesis, and Biofilm Formation

Joshua A. Visser,[a] Deborah Yager,[a] Schuyler A. Chambers,[a] Ji Youn Lim,[a] Xujun Cao,[a] and Lynette Cegelski[a]*

[a] Dr. Joshua A. Visser, Dr. Deborah Yager, Dr. Schuyler A. Chambers, Dr. Ji Youn Lim, Mr. Xujun Cao, Prof. Lynette Cegelski
Department of Chemistry
Stanford University
380 Roth Way, Keck Building, Stanford, CA 94305
E-mail: cegelski@stanford.edu

Supporting information for this article is given via a link at the end of the document.

Abstract: *Escherichia coli* and other Enterobacteriaceae thrive in robust biofilm communities through the coproduction of curli amyloid fibers and phosphoethanolamine cellulose. Curli promote adhesion to abiotic surfaces and plant and human host tissues and are associated with pathogenesis in urinary tract infection and food-borne illness. As amyloid, curli production in the host has also been implicated in the pathogenesis of neurodegenerative diseases. We report that the natural product nordihydroguaiaretic acid (NDGA) is effective as a curlicide in *E. coli*. NDGA prevents CsgA polymerization *in vitro* in a dose-dependent manner. NDGA selectively inhibits cell-associated curli assembly and inhibits uropathogenic *E. coli* biofilm formation. More broadly, this work emphasizes the ability to evaluate and identify bioactive amyloid assembly inhibitors using the powerful gene-directed amyloid biogenesis machinery in *E. coli*.

Introduction

E. coli is a model organism for bacterial genetics and cell biology and is widely recruited in biotechnology efforts to produce proteins and other biomolecules, usually using selected strains that grow rapidly and are deficient in aggregative phenotypes.[1] *E. coli* are also commonly present as commensal organisms in the human and animal gastrointestinal tract as part of the microbiome. Yet, *E. coli* emerge as pathogens and cause disease in humans, animals, and plants. In particular, *E. coli* can compromise gut epithelial barriers and lead to intestinal inflammation that is linked to inflammatory bowel diseases, *e.g.* Crohn's disease and ulcerative colitis.[2,3] *E. coli* can exit the GI tract and move to ascending infections of the urinary tract, causing infections of the bladder (cystitis) and kidneys (pyelonephritis).[4] *E. coli* as well as *Salmonella* species can also colonize plant tissue, such as alfalfa, lettuce and spinach leaves, and adhere to abiotic surfaces in food processing environments, leading to food-borne disease in humans who ingest contaminated plant material.[5,6]

E. coli rely on the production of numerous types of adhesive proteins, fibers, and polysaccharides to facilitate host colonization and persistence.[7–10] *E. coli* also thrive in the environment and in the host as adherent bacterial communities termed biofilms.[11,12] Bacterial biofilms are surface-associated communities of bacteria typically encapsulated in a self-produced extracellular matrix (ECM).[13] *E. coli* can adhere to different types of substrates depending on the specific adhesive proteins or polysaccharides they present at their cell surface and can assemble different types of biofilm communities that depend on the molecular composition of their extracellular matrix.[7–10] Many commensal strains and pathogenic strains of *E. coli* form distinctive biofilms specifically through the co-production of functional amyloid fibers termed curli and a cellulosic component,[14,15] which we recently discovered is a chemically modified form of cellulose – phosphoethanolamine (pEtN) cellulose.[16] These *E. coli* elaborate highly wrinkled macrocolony architectures when grown from a single drop of inoculum, typically on low-salt nutrient agar.[15,17] Curli were first identified as bacterial fibers in 1989[18] and were later revealed to be amyloid fibers (2002),[19] providing the first identification of a bacterial amyloid. Cegelski and Hultgren and coworkers demonstrated curli's influence in conferring a fitness advantage to bacteria *in vivo* in the murine cystitis model and identified the first small molecule inhibitors of curli assembly, termed curlicides, which inhibited *E. coli* biofilm formation.[20] Curliated *E. coli* are highly prevalent among clinical isolates associated with pyelonephritis and the production of curli is strongly correlated with the progression of UTI to sepsis.[21,22] More recent work revealed the molecular interplay of curli and pEtN cellulose in enabling adhesion to bladder epithelial cells.[23] In conditions of high shear, pEtN cellulose was required for curli association at the bacterial cell surface and for strong attachment to the mammalian cell monolayer, revealing a type of Velcro or mortar-like role for pEtN cellulose, facilitating curli to mediate strong adhesion to bladder epithelial cells in the absence of other adhesins such as type 1 pili.[23] Beyond adhesion, curli induce immune activation of Toll-like receptors and the CD4 complex, and are responsible for the production of proinflammatory cytokines.[24–26]These factors additionally contribute to curli's influence on pathogenesis *in vivo*.[20,24,27] Furthermore, beyond the realm of traditionally considered infectious disease, there is a growing number of studies that underscore the possible influences of bacterial amyloids produced in the host in neurodegenerative diseases, specifically Alzheimer's and Parkinson's diseases, as well as in autoimmune disorders.[28–32] At the same time and juxtaposed to the emphasis on the deleterious consequences of curli production, the cellulosic polysaccharide has been shown to reduce curli-associated antigenicity, perhaps by masking curli recognition by the immune system.[27,33–35] Thus, methods to manipulate the

production of curli and/or pEtN cellulose provide tools to study this complex interplay. Inhibitors of curli, in particular, may also hold value in inhibiting bacterial-mediated pathogenesis in these human disorders.

Curli assembly in *E. coli* requires the coordination of several proteins that make up the curli amyloid assembly machinery to properly direct the nucleation and polymerization of CsgA into amyloid fibers at the cell surface.[19] CsgG is an outer membrane protein that assembles into a multimeric secretion pore through which curli subunits CsgA and CsgB and the chaperone-like protein CsgF are transported.[36–40] CsgB is the nucleator protein which stays cell-associated after transport through CsgG and serves to nucleate CsgA.[19,41] CsgE is a type of gatekeeper protein influencing curli subunit secretion through CsgG.[42,43] Thus, there are many opportunities to interfere with curli biogenesis. Since amyloid polymerization occurs outside the cell through this nucleation-precipitation machinery, we are presented with the opportunity to inhibit curli and biofilm formation outside the cell, without requiring molecules to enter cells. We identified the first small-molecule curlicide, a ring-fused 2-pyridone, termed FN075, through cell-based *E. coli* screening of a small library of about 20 synthetic ring-fused pyridones that were inhibitors of the *in vitro* polymerization of the eukaryotic protein β-amyloid into amyloid.[20] Many inhibitors that were competent as inhibitors of amyloid using purified proteins *in vitro* were not potent in inhibiting cell-based curli assembly. FN075 was a stand-out compound and was potent in inhibiting curli biogenesis in growing bacteria. [20] It inhibited *in vitro* polymerization of the major curli subunit, CsgA, as evaluated through Thioflavin-T (ThT) fluorescence assays, categorizing it as a curlicide or curli assembly inhibitor.[20] Since the identification of FN075, additional curlicides have been reported, including new 2-pyridone compounds[44]; and parthenolide and a benzoquinone derivative[45].

We sought to examine the possible potency of the natural product nordihydroguaiaretic acid (NDGA)[46] to inhibit curli biogenesis, inspired by its wide study in eukaryotic amyloid systems. NDGA has been reported to inhibit the *in vitro* oligomerization and fibril formation of Aβ-40 and Aβ-42 peptides[47–49] associated with Alzheimer's disease and inhibit polymerization of α-synuclein associated with Parkinson's and other neurodegenerative diseases[50,51]. NDGA is a natural product, contributing up to 15% of the dry mass of the leaves of the Creosote bush, *Larrea tridentate*.[56] The creosote bush is commonly found in the desert areas of the southwestern U.S. and northern Mexico[56] and has a long history of use in traditional medicines.[57] NDGA contains a biphenolic chemical scaffold similar to other molecules that bind amyloids, such as Congo red (Figure 1A).[52] However, in *E. coli*, Congo red binds curli and serves as an indicator dye, but does not inhibit curli biogenesis or biofilm phenotypes[53,54] [41,55]. Here, we report our discovery and characterization of NDGA as a curlicide and curli-associated biofilm inhibitor.

Results and Discussion

NDGA inhibits CsgA polymerization *in vitro*.

We hypothesized that NDGA would inhibit the polymerization of purified soluble CsgA into amyloid fibers given its ability to inhibit polymerization and amyloid formation of human amyloidogenic proteins, specifically α-synuclein [50,51] and Aβ-40 and Aβ-42 peptides[47–49]. We tested this hypothesis using two biochemical assays. First, we employed a conventional *in vitro* Thioflavin T (ThT) detection-based CsgA amyloid polymerization assay.[58]

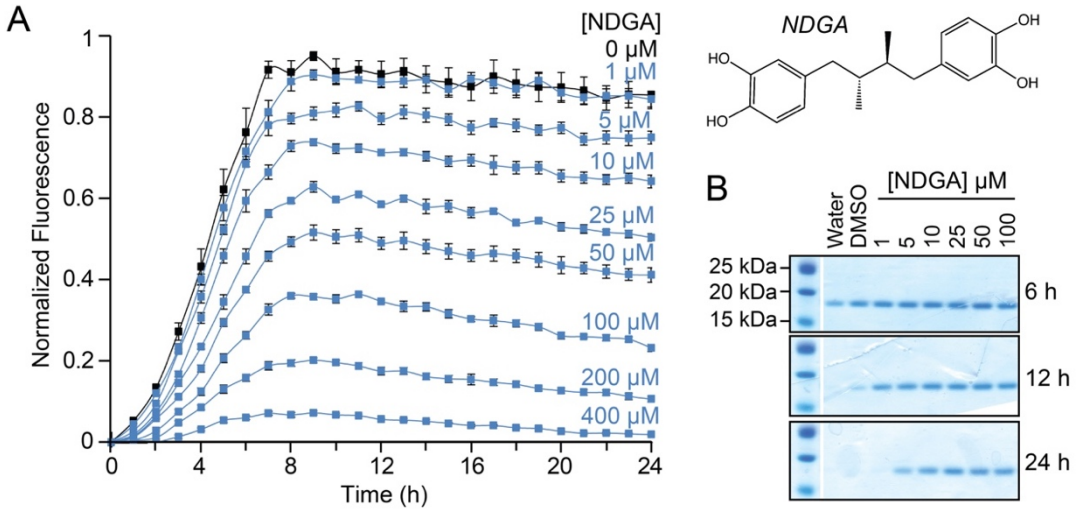

Figure 1. NDGA inhibits polymerization of CsgA. (A) Purified His_6-CsgA incubated with specified concentrations of NDGA in the presence of ThT revealed a dose-dependent reduction in ThT fluorescence intensity, with measurements made from the time of mixing through 24 hours. Data (squares) represent the mean of 6 technical replicates and error bars represent the standard deviation and are within the squares in some cases. The plot is representative of results from 3 biological replicates. ANOVA and Tukey's test of 24-hour measurement indicated no statistical significance between 0 and 1 μM NDGA treatment, whereas every other paired comparison is statistically significant with $p<0.01$. (B) His_6-CsgA incubated with NDGA revealed an increase in observed SDS-soluble CsgA species, directly demonstrating the inhibition of amyloid assembly, while polymerization ensued for non-treated CsgA, leading to SDS-insoluble structures. Densitometry analysis is provided in Figure S1. The 14kD CsgA appears between 15-20 kD by SDS PAGE.[19]

Histidine-tagged CsgA (His_6-CsgA) was purified in a soluble, unstructured form and incubated at room temperature at a concentration of 10 μM in the presence of NDGA (compound characterization in Figure S1). Incubation of 10 μM CsgA with 1 μM NDGA was not effective, whereas a dose-dependent decrease in ThT fluorescence intensity was observed for CsgA treated with NDGA concentrations of 5 μM and greater (Figure 1A). 25 μM NDGA (NDGA-to-CsgA molar ratio of 2.5) yielded a reduction in final ThT fluorescence by more than 50%. Fluorescence was nearly completely eliminated during the time-course for treatment with 400 μM NDGA (Figure 1A). Analysis of variance (ANOVA) and Tukey's test indicated no statistical significance between the 24-hour endpoint measurements for 0 and 1 μM NDGA treatment, whereas the differences for all other paired comparisons are statistically significant with $p<0.01$. Overall, inhibition in curli-associated ThT fluorescence is consistent with inhibition of CsgA polymerization.

We included further characterization to more directly evaluate the polymerization status of CsgA over time using SDS-PAGE analysis, wherein CsgA present as amyloid fibers does not enter the SDS-PAGE gel unless treated with formic acid or hexafluoroisopropanol to solubilize CsgA (as in Figure 1B). Any detection of monomeric CsgA in the protein gel is indicative of SDS-soluble CsgA that has not assembled into amyloid. Beyond 6 hours, diminution of CsgA was observed for the untreated control as CsgA polymerization ensued (Figure 1B). CsgA incubated with NDGA revealed increases in SDS-soluble CsgA for samples examined at 12- and 24-hour treatment times for concentrations as low as 5 μM NDGA, which represents a two-fold molar excess of CsgA over NDGA (Figure 1B). Densitometry analysis for band intensities is provided in Figure S2. Thus, direct detection of CsgA by protein gel analysis confirmed that NDGA inhibited polymerization of CsgA into SDS-insoluble fibers.

NDGA reduces whole-cell curliation and does not influence curli gene transcription.

We next examined whether the ability of NDGA to inhibit polymerization of CsgA *in vitro* would translate into efficacy in preventing CsgA polymerization at the bacterial cell surface for growing *E. coli*. The influence of NDGA on cell-associated curli levels was evaluated through western blot analysis. Bacteria were grown on NDGA-supplemented YESCA agar plates, and harvested bacteria were normalized by cell density to compare whole cell curliation. To facilitate reliable quantification of cell density and analysis of CsgA, we used the laboratory strain MC4100 to obtain whole-cell suspensions. MC4100 is the well-studied curli-producing *E. coli* strain in which most studies involving curli biogenesis have been reported.[58–60] MC4100 does not produce pEtN cellulose and thus does not exhibit aggregation associated with other biofilm-forming strains such as UTI89 and is ideally suited to interrogate curli-specific phenomena. A reduction in cell-associated CsgA was observed for NDGA-treated MC4100 (Figure 2A), whereas CsgG and CsgF levels were unaffected. CsgB was unaffected through 100 μM. A reduction in cell-associated CsgB was observed at 100 μM NDGA. The western blots for all four proteins were performed on the same whole cell sample treated with formic acid to solubilize CsgA. CsgA (14 kD) and CsgG (30 kD) differ by mass and were probed from the same western blot sliced between the two. Separate gels were run for CsgE and CsgF which run similarly to CsgA. Overall, the detection of curli assembly proteins is supportive that the curli secretion machinery is not disrupted and the reduction in CsgA is consistent with the activity of an amyloid assembly inhibitor.

We hypothesized that NDGA was operating as a curlicide, or assembly inhibitor, and not through inhibition of gene expression, although inhibitors can exhibit multiple modes of action. Thus, we next sought to determine whether NDGA exerted any significant effect on transcription of curli genes through qRT-PCR analysis. Results from qRT-PCR for cells grown for 24 hours indicated that expression levels of all curli proteins (*csgA, csgB, csgD, csgE, csgF,* csgG) were comparable for untreated and NDGA-treated cells (Figure 2B). There was no significant difference at a threshold $p < 0.01$. Expression of *rpoS*, a major subunit of RNA polymerase, was also not affected by NDGA treatment within the

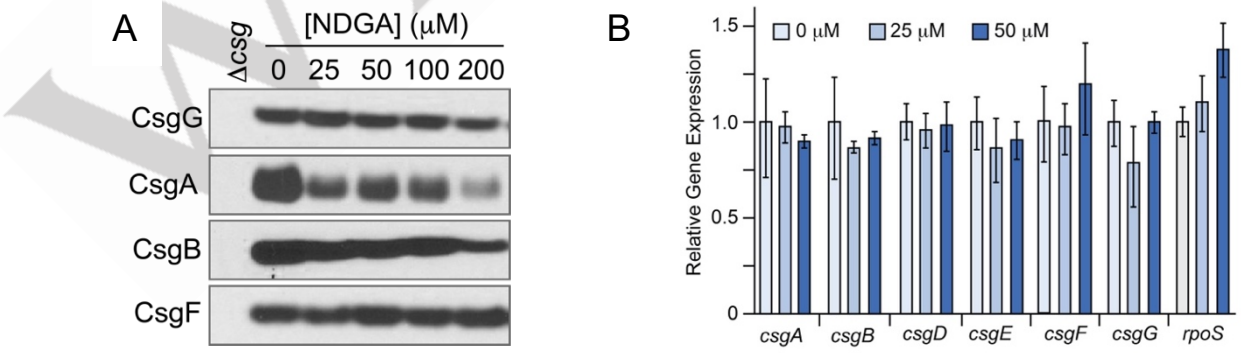

Figure 2. Whole-cell curliation is reduced without reduction in gene transcription. (A) Whole-cell western blot analysis indicated a reduction in the major curli protein CsgA without an effect on CsgG or CsgF after growth for 48 hours. A small reduction in CsgB is observed at 200 μM NDGA. Western blots are representative of 2-3 biological replicates. (B) Quantification of mRNA levels by qRT-PCR of bacteria grown for 24 hours revealed that NDGA (concentrations of 0, 25, and 50 μM) exhibited no inhibition of transcription of curli genes (mean values +/- standard deviation). Expression of the master regulator *rpoS* was assessed for comparison.

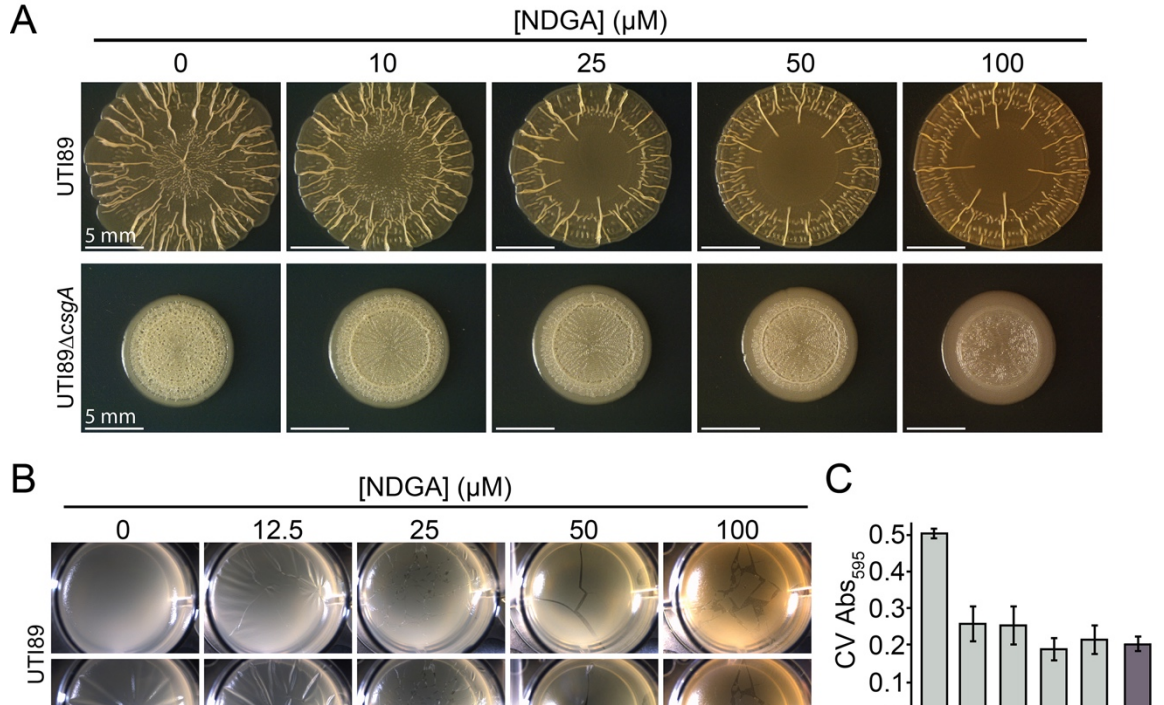

Figure 3. NDGA inhibits biofilm phenotypes. (A) The macrocolony wrinkling phenotype of UTI89 grown on NDGA-supplemented YESCA agar for 72 hours was suppressed for all NDGA concentrations. Images are representative of results from 3 biological replicates. (B) UTI89 pellicle formation in 12-well-plate wells with 4 mL culture volume was inhibited in a dose-dependent manner when grown in the presence of NDGA and documented at 72 hours. Images are representative of results from 3 biological replicates. (C) NDGA supplementation in YESCA nutrient broth resulted in reduced biomass accumulation of UTI89 to walls of PVC 96-well plates, as evaluated by crystal violet staining. Data represent mean +/- standard deviation for 6 technical replicates. One-way ANOVA analysis and Tukey's test indicates statistical significance ($p<0.01$) between 0 μM NDGA treatment compared with each other group. There is no statistically significant difference between other groups by the Tukey test. Experimental results are representative of two biological replicates.

same bounds. RpoS is the master regulator of stationary gene expression in *E. coli*.[61] Typically, in *E. coli*, changes in mRNA levels above or below a factor of 1.5 to 2.0 are considered biologically significant, with p values of $p < 0.01$.[62–64] Thus, NDGA did not influence curli gene expression.

NDGA inhibits macrocolony architecture, pellicle formation, and plastic-associated biofilm formation.

E. coli elaborate highly wrinkled macrocolony architectures on nutrient agar when they coproduce curli and pEtN cellulose.[15,20] We moved from the above analysis of curli production by a curli-only producer to examine the ability of NDGA to alter UTI89 macrocolony architecture and other biofilm community phenotypes which require co-production of curli and pEtN cellulose.[20] For the evaluation of macrocolony architecture, the uropathogenic *E. coli* strain UTI89 was grown on YESCA agar supplemented with varied concentrations of NDGA for 72 hours at 26 °C. NDGA supplementation resulted in a reduction in the extent of wrinkling, suggesting that the production of extracellular matrix was perturbed (Figure 3A). Wrinkling was most notably altered with NDGA treatment concentrations at and above 25 μM. Some wrinkling was still observed at 100 μM. The inhibition of UTI89 macrocolony architecture was also observed among a panel of *E. coli* clinical isolates previously reported as biofilm formers producing both curli and pEtN cellulose[65] and for *Salmonella enterica* serotype Typhimurium (*S.* Typhimurium) which similarly produces curli and pEtN cellulose (Figure S3)[15,16]. This comparative analysis demonstrated that the influence of NDGA on macrocolony architecture is not limited to a single strain. Macrocolony architecture was also documented for UTI89 curli and pEtN cellulose mutants. UTI89Δ*csgA*[20] lacks curli and produces pEtN cellulose and typically exibits a subtle puckering across the macrocolony, although it is a more variable phenotype than for UTI89. Inhibition of puckering at the outer rim of the macrocolony was observed at 100 μM NDGA and manifest to a lesser extent at 25 nd 50 μM NDGA. Macrocolonies of the mutants UTI89Δ*bcsA*[23], and UTI89Δ*csgA*Δ*bcsA*[23] do not exhibit any texture and appear smooth. Growth on NDGA-supplemented agar did not alter the smooth macrocolonies (Figure S4).

We next evaluated the influence of NDGA on the formation of biofilms at the air liquid interface, termed pellicles. The coproduction of curli and pEtN cellulose enables bacteria to adhere to the sides of multi-well plate wells with the accumulation of cells and biomass across the surface of the liquid phase nutrient medium, forming a pellicle.[20] Pellicle formation was evaluated in a 12-well plate format with 4 mL culture volumes of UTI89 in the absence and presence of varied concentrations of NDGA (Figure 3B). We expected to observe a reduction in pellicle

formation, as observed for previously reported curlicides.[20,66] Indeed, we observed a weakening of the pellicle with as low as 12.5 μM NDGA, with the pellicle exhibiting holes and tears at concentrations of 25 μM and 50 μM, respectively. Perturbations were observed at lower concentrations of NDGA in this broth-based pellicle assay than in the agar-based microcolony assay. This is often observed and, at least in part, can be attributed to the ready diffusion of compound in broth as compared to the more abrupt local depletion of compound that occurs in the semi-solid agar phase assay, reducing available compound as cells grow. UTI89Δ*bcsA* is capable of forming pellicle-like aggregates at the air-liquid interface due to the production of curli and these fragile pellices are also interrupted for cells grown in the presence of NDGA (Figure S5). UTI89Δ*csgA* and UTI89Δ*csgA*Δ*bcsA* do not form appreciable pellicles and these are unchanged in the presence of NDGA (Figure S5).

NDGA was additionally evaluated for its ability to influence bacterial adhesion and biomass accumulation on plastic in a traditional 96-well plate crystal violet assay. In this assay, bacteria are grown to permit adhesion and biofilm formation within wells, after which non-adherent bacteria are washed away and the extent of biomass accumulation is documented through crystal violet staining [67,68] and quantification of the biomass-associated crystal violet through ethanol dissolution and UV-Vis spectrophotometry[69]. In this format, NDGA resulted in a loss of adhesion starting at concentrations as low as 2.5 μM (Figure 3C). The diminution yields comparably low background level staining as the curli deficient strain UTI89Δ*csgA*. These results complement those obtained for pellicle formation, demonstrating that NDGA inhibits curli-dependent adhesion and biofilm formation. Thus, NDGA inhibits curli-dependent biofilm formation on plastic, on agar, and at the air-liquid interface.

NDGA does not exert an influence on pEtN cellulose production.

The production of biofilms as described above are indeed curli-dependent, yet they are also dependent on the production of pEtN cellulose. Thus, we further considered whether NDGA additionally had any influence on the production and cell-association of pEtN cellulose. To determine if NDGA treatment resulted in any influence on pEtN cellulose production, we employed two dye-based assays. We employed a traditional Calcofluor based assay[70] and our recently introduced method based on the distinguishing Congo red-associated fluorescence of bacteria producing pEtN cellulose[71] to evaluate production of pEtN cellulose by cells grown in the presence of NDGA (Figure 4A). Calcofluor-based fluorescence is useful and commonly employed, but is used only qualitatively to detect major changes to the production of polysaccharides and is not used quantiatively.

For untreated pEtN cellulose-producing controls, UTI89Δ*csgA* also always exhibits greater Calcoflour-associated fluorescence than the wild type UTI89, which is attributed to the greater access of pEtN cellulose to the dye in the absence of pEtN cellulose interactions with curli.[71] Comparable Calcofluor-associated

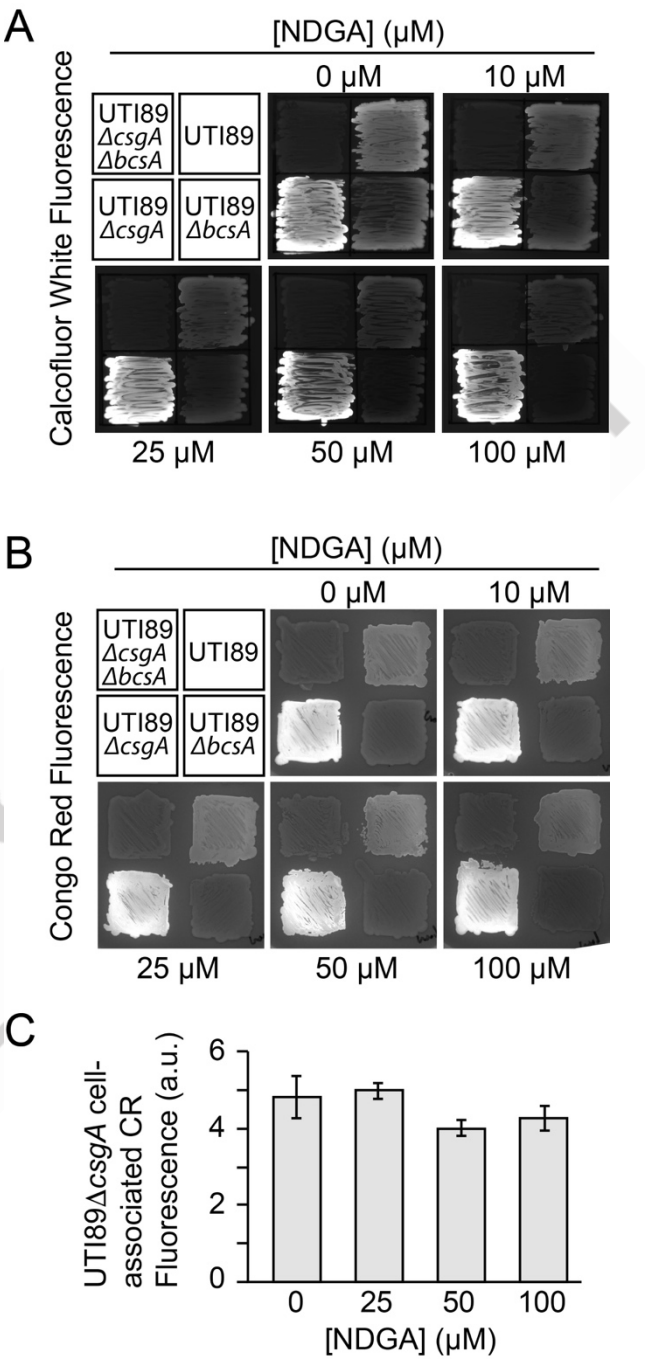

Figure 4. NDGA does not influence pEtN cellulose production. (A) Calcofluor-associated fluorescence was maintained across NDGA concentrations as documented at 48 hours, noting that UTI89Δ*csgA* lacks curli and thus exhibits brighter Calcofluor fluorescence and is an ideal strain for monitoring possible alterations in pEtN cellulose production. Images are representative of 3 biological replicates. (B) Congo red-associated fluorescence was maintained for growth in YESCA supplemented with NDGA and grown for 48 hours. Images are representative of 3 biological replicates. (C) Bacterial cell suspensions of cells grown on YESCA plates supplemented with NDGA and harvested into Tris buffer containing 3 μg/mL Congo red also revealed comparable levels of Congo red fluorescence, supporting similar production levels of pEtN cellulose. The mean +/- standard deviation of 3 technical replicates is presented for one of two biological replicates.

fluorescence was observed for the respective pEtN cellulose producers, UTI89Δ*csgA* and UTI89, in the absence of NDGA and when grown on NDGA-supplemented agar with no marked reductions or differences (Figure 4A).

The Congo red fluorescence assay adds power to results from the Calfofluor-based assay as it can distinguish between whether UTI89 is producing pEtN cellulose or unmodified cellulose, whereas both would exhibit Calcofluor fluorescence. (Figure 4B). Congo red exhibits strong fluorescence when bound to modified pEtN cellulose, well above that of Congo red bound to curli or unmodified cellulose.[71] In the absence of NDGA treatment, UTI89Δ*csgA* always exhibits the greatest Congo red-associated fluorescence, whereas the coproduction of curli with pEtN cellulose in wild type UTI89 serves to dampen the observed fluorescence, similar to that observed for Calcofluor-associated fluorescence[71] (Figure 4B). The pEtN cellulose mutants, UTI89Δ*bcsA* and UTI89Δ*bcsA*Δ*csgA* were devoid of notable Congo red-associated fluorescence, as expected. NDGA did not detectably impact Congo red fluorescence for either UTI89 or UTI89Δ*csgA*, suggesting that NDGA did not inhibit pEtN cellulose production (Figure 4B).

In order to more quantitatively examine the possible influence of NDGA on pEtN cellulose, we also employed a complementary and semi-quantitative Congo red fluorescence assay, which is applicable to harvested cells in suspension that are not coproducing curli.[71] UTI89Δ*csgA* cells were grown on YESCA agar containing NDGA and then incubated with Congo red, followed by fluorescence measurements of each cell suspension. We observed comparable fluorescence for samples treated with NDGA at concentrations of 10 μM to 100 μM (Figure 4C). Thus, no major change to pEtN cellulose production was attributed with NDGA treatment. Our collective results demonstrate that NDGA is a curlicide. NDGA prevents curli biogenesis in growing bacteria and prevents curli-associated biofilm phenotypes.

Conclusion

E. coli and other Gram-negative bacteria harbor dedicated genetic and molecular machinery to assemble curli amyloid fibers at the cell surface. Together with curli, *E. coli* and *Salmonella* species often co-produce phosphoethanolamine cellulose, resulting in distinctive tissue-like biofillm architectures, including wrinkled macrocolonies when grown on agar. The production of curli is associated with bacterial pathogenesis and is a trigger for inflammation, implicated in chronic inflammatory diseases.[21-35] Strategies to inhibit curli production have potential in ameliorating disease pathogenesis. We discovered that NDGA inhibited CsgA polymerization *in vitro*, inhibited curli biogenesis in *E. coli*, and prevented biofilm formation by pathogenc bacteria. NDGA's activity in inhibiting curli assembly is juxtaposed to the influence of Congo red which binds curli but does not inhibit curli assembly at the cell surface.[53] We hypothesize that NDGA is capable of recognizing intermediate amyloidogenic conformations of CsgA en route to amyloid formation, whereas Congo red recognizes β-strand amyloid epitopes (as well as polysaccharide structures, including celluloses). NDGA may prove valuable in structural and biophysical investigations to examine potentially capped CsgA subunits or small assemblies, CsgA-pEtN cellulose assemblies, and possibly other microbial amyloid-forming proteins. Our work builds on a larger body of work that has identified naturally produced small molecules and external stimuli that influence curli gene expression and/or amyloid assembly, such as human bile acids and common plant flavonoids.[73-75] The influence of NDGA as a curlicide underscores the importance of considering the influence of small molecules present around bacterial communities in the host, such as in the gastrointestinal tract and in the environment. Given the implications of curli as mediators of inflammation and potential contributors to neurogenerative diseases, NDGA or even more potent analogs could be of value in preventing curli assembly in the host towards the prevention of human disease. Furthermore, *E. coli* more generally presents us with a highly efficient gene-directed and tightly controlled amyloid assembly machinery as a powerful platform in which to evaluate and identify the most potent bio-active inhibitors of CsgA and potentially other amyloid proteins in a tractable cellular context.

Experimental Section

Bacterial Strains and Growth Conditions

The UPEC strain UTI89, the curli mutant UTI89Δ*csgA*, cellulose mutant UTI89Δ*bcsA*, double mutant UTI89Δ*csgA*Δ*bcsA,* as well as the laboratory strain MC4100 and the full curli gene mutant, MC4100Δ*csg,* were used to evaluate curli formation, biofilm formation, and the influence of small-molecule inhibitors. These bacterial strains were typically grown on YESCA agar (1 g/L yeast extract, 10 g/L casamino acids) at 26 °C. The complete curli deletion mutant LSR12[36] in the C600 *E. coli* background was used for *in vitro* CsgA assays along with the plasmids pMC1[19] and pMC3[19] that encode CsgG and His_6-tagged CsgA, respectively. Transformed LSR12/pMC1/pMC3 was grown in LB broth (10 g/L bacto tryptone, 5 g/L yeast extract, and 10 g/L sodium chloride) supplemented with 100 μg/mL ampicillin and 25 μg/mL chloramphenicol to maintain the plasmids. NDGA (≥ 97% purity) was purchased from Sigma-Aldrich (74540). Calcofluor White MR or Fluorescent Brightener 28 was purchased from Sigma-Aldrich (F3543) and Congo red was purchased from MP Biomedicals, LLC. For supplementation of plates with NDGA, a 100 mM NDGA stock solution was prepared in DMSO. Appropriate volumes were added to agar medium after autoclaving and upon cooling of agar medium to ~55 °C.

His_6-CsgA Purification for in vitro Polymerization Experiments

His_6-tagged CsgA was produced and purified as previously reported.[58] Briefly, LSR12 was transformed with pMC1 and pMC3 plasmids, encoding CsgG and His_6-tagged CsgA, respectively. 30 mL of overnight culture was added to 1L of LB-Amp/Cm broth and incubated at 37 °C with shaking to reach an

approximate OD_{600} of 1. This culture was induced with 1 mL of 250 mM IPTG (for a final concentration of 0.25 mM IPTG) to promote *csgA* expression and cells were allowed to grow for an additional 45 minutes. Cells were centrifuged at 10,000 x g for 15 min at 4 °C. The supernatant was retained and filtered through a 0.22 µm polyethersulfone bottle-top filter (Millipore Sigma no. S2GTP05RE), passed over a Ni-NTA (Thermo Fisher No. 88222) Kontes column, and washed with 50 mM potassium phosphate. CsgA was eluted using 50 mM potassium phosphate containing 100-200 mM imidazole. Buffer exchange was then performed using 7 kD molecular weight cut-off spin desalting columns (Thermo Scientific No. 89892) to remove imidazole in preparation for polymerization experiments.

Thioflavin T Detected Polymerization Assay

10 µM of purified His_6-CsgA was incubated with 20 µM Thioflavin T and specified concentrations of NDGA (total [DMSO] = 0.1%) in black 96-well plates with clear bottoms (Corning No. 3603) for 24 h with shaking at room temp for 3 s before each read. Fluorescence measurements were taken every twenty minutes with λ_{ex} of 438 nm, λ_{em} of 495 nm, and cut-off at 475 mm using a SpectraMax M5 spectrometer (Molecular Devices).

Biochemical Protein Gel-Based Analysis of CsgA Polymerization

200 µL of 15.9 µM His_6-tagged CsgA was added to 5 mL polystyrene culture tubes (Falcon No. 352058). To the tubes was added specified concentrations of NDGA (total [DMSO] = 0.4%) and Tween 20 to a concentration of 0.0001% v/v to prevent adhesion of protein to the walls of the tube. Aliquots were taken at time points given and suspended 1:1 in SDS-PAGE loading buffer and run on 4-12% Bis-Tris SDS-PAGE gels (Invitrogen). PAGE gels were stained with Coomassie blue. Molecular weight markers are Bio-Rad Model 1610374 (Precision Plus Protein Dual Color Standards).

Western Blot Assay

Cell-associated curli proteins CsgA, CsgB, CsgF, and CsgG were examined by immunoblot assays. MC4100 and MC4100Δ*csg* were grown as lawns on YESCA agar supplemented with specified concentrations of NDGA and with a final DMSO concentration of 0.4% in each sample for 24 hours. Cells were harvested and resuspended in 1 mL of PBS and prepared as cell pellets with an optical density at 600 nm (OD_{600}) of 1.0. Each pellet was treated with 100 µL of formic acid to dissociate CsgA subunits. Formic acid was removed by vacuum centrifugation, and samples were resuspended in 200 µL of sodium dodecyl sulfate-polyacrylamide gel electrophoresis (SDS-PAGE) loading buffer. Protein gel electrophoresis was carried out using 12% SDS-PAGE gels (Invitrogen) and proteins were transferred to 0.2 µm pore size nitrocellulose transfer membranes (Whatman). After transfer, membranes were stained with Ponceau S (Amresco no. K793) for visualization of total protein levels. Polyclonal rabbit antiserum to a CsgA peptide (CGNGADVGQGSDDSS), CsgB peptide (CEGSSNRAKIDQTGDY), CsgG peptide (DGIDRGLWDLQNKAERQND), and purified His_6-tagged CsgF protein[39] was used as the primary antibodies, and horseradish peroxidase (HRP)-conjugated goat anti-rabbit antibody (Pierce) was used as the secondary antibody. Signal was developed using SuperSignal West substrate.

Quantitative Real-Time PCR

Transcription of curli genes was examined by qRT-PCR. As described previously[72], colonies were inoculated as four 15 µL aliquots of overnight cultures on YESCA agar plates containing various concentrations of NDGA (with final DMSO concentration of 0.2%) and grown for 12 and 24 hours. The RNA was stabilized using RNAprotect Bacteria Reagent (Qiagen No. 76506) and then isolated using the RNeasy Mini Kit (Qiagen No. 74104). Synthesis of cDNA was performed using the High-Cpacity cDNA Reverse Transcription Kit (Applied Biosystems No. 4368814). Real-time PCR measurements were performed on the Applied Biosystems StepOne Plus system using QuantiFast SYBR Green PCR Kit (Qiagen No. 204054). The ΔΔCT method[76] was used for analysis of the qRT-PCR data, using bacteria grown without compound as the reference sample. All cDNA levels were normalized to levels of *rrsH* (16S rRNA) from the same sample.

Agar Macrocolony Assay

Agar-based macrocolony architectures were evaluated on agar plates, wherein bacterial growth was initiated by spotting 10 µL of an overnight starter culture of UTI89 and UTI89Δ*csgA* onto each YESCA agar plate with specified concentrations of NDGA. Macrocolonies were observed after 48 or 72 hours of growth as indicated and documented using a Leica S6D Stereomicroscope and camera.

Pellicle Assay

Pellicle formation was initiated by inoculating 4 µL of an overnight starter culture of UTI89 in 4 mL of YESCA broth in 12-well plates containing specified concentrations of NDGA and incubated at 26 °C for 48 hours. One quarter of the media was replaced after 24 hours of growth, containing a fresh bolus of compound. Pellicle formation was inspected visually and photographed.

PVC-associated Biofilm Assay

Overnight cultures of UTI89 and UTI89Δ*csgA* were diluted to OD_{600} = 0.5 using sterile PBS. 690 µL of this dilute culture was added to 10 mL of YESCA broth and aliquoted. To each aliquot was added specified concentrations of NDGA (total [DMSO] = 0.2%). 150 µL of each sample was added to 6 wells of a 96-well polystyrene microtiter plate (Costar No. 3370). Plates were incubated at 26 °C for 48 h of growth with 1 min of shaking at 200 rpm every 20 minutes. Wells were rinsed and stained with crystal violet (Sigma-Aldrich No. C3886). Specifically, 170 µL of 0.1% crystal violet was added to each well and incubated for 45 minutes at room temperature. The bulk crystal violet solution was removed,

and each well was washed three times with 170 µL of water. The adherent crystal violet was then dissolved with 170 µL of 95% ethanol for 30 minutes at 4 °C. 100 µL of each well was transferred to a polystyrene microtiter plate, and absorbance was measured at 595 nm in a microplate reader (SpectraMax M5, Molecular Devices).[69]

Calcofluor and Congo Red Fluorescence of Agar-grown Cells and Congo Red Fluorescence of Cell Suspensions

As previously described[74] bacterial cells were grown on YESCA agar containing 10 µg/mL Calcofluor White or 25 µg/mL Congo red at 26 °C for 48 h of growth. Bacterial lawns were visualized directly by eye and for fluorescence. Calcofluor plates were imaged using the Azure 400 Digital Imager with UV-light excitation and Congo red plates were imaged using a Bio-Rad ChemiDoc imager. Semi-quantitative detection of Congo red-associated fluorescence of pEtN cellulose producing bacteria was performed as previously described. [74] Briefly, bacterial cells were grown on YESCA agar at 26 °C for 24 h and harvested into 10 mM Tris (pH 7.4). Cell suspensions for each condition were normalized to an optical density (OD) of 4 and serially diluted to ODs of 3, 2, and 1. CR (1 mg/mL) was added to 1 mL of each bacterial suspension to give a final concentration of 3 µg/mL. 200 µL of each suspension was added in triplicate to a 96-well plate (Corning No. 3603). Fluorescence measurements were performed using λ_{ex} of 525 nm and λ_{em} of 610 nm on a SpectraMax M5 spectrometer (Molecular Devices).

Supporting Information

The authors include Supporting Figures and Supporting Experimental Procedures in Supporting Information.

Acknowledgements

This material is based upon work supported by the National Science Foundation Award 2001189 (L.C.). and prior NSF CAREER/PECASE Award 1453247 (L.C.). The authors thank Prof. Matt Chapman for plasmids for His_6-tagged CsgA production. The authors thank Prof. Ed Krol for valuable discussion.

Keywords: Natural products • Peptides • Protein-protein interactions • Amyloid • Biofilm inhibitor

References

[1] Z. D. Blount, *Elife* **2015**, *4*, DOI 10.7554/eLife.05826.
[2] R. J. Xavier, D. K. Podolsky, *Nature 2007 448:7152* **2007**, *448*, 427–434.
[3] C. Palmela, C. Chevarin, Z. Xu, J. Torres, G. Sevrin, R. Hirten, N. Barnich, S. C. Ng, J. F. Colombel, *Gut* **2018**, *67*, 574–587.
[4] R. D. Klein, S. J. Hultgren, *Nature Reviews Microbiology 2020 18:4* **2020**, *18*, 211–226.
[5] C. N. Berger, S. V Sodha, R. K. Shaw, P. M. Griffin, D. Pink, P. Hand, G. Frankel, *Wiley Online Library* **2010**, *12*, 2385–2397.
[6] A. Bridier, P. Sanchez-Vizuete, M. Guilbaud, J. C. Piard, M. Naïtali, R. Briandet, *Food Microbiol* **2015**, *45*, 167–178.
[7] S. J. Hultgren, S. Abraham, M. Caparon, P. Falk, J. W. S. Geme, S. Normark, *Cell* **1993**, *73*, 887–901.
[8] L. Cegelski, C. L. Smith, S. J. Hultgren, *Encyclopedia of Microbiology* **2019**, 93–102.
[9] J. Mainil, *Vet Immunol Immunopathol* **2013**, *152*, 2–12.
[10] P. Klemm, M. A. Schembri, *International Journal of Medical Microbiology* **2000**, *290*, 27–35.
[11] Di. O. Serra, R. Hengge, *https://doi.org/10.1146/annurev-micro-031921-055801* **2021**, *75*, 269–290.
[12] E. Rossi, A. Cimdins, P. Lüthje, A. Brauner, Å. Sjöling, P. Landini, U. Römling, *https://doi.org/10.1080/1040841X.2017.1303660* **2017**, *44*, 1–30.
[13] L. Hall-Stoodley, J. W. Costerton, P. Stoodley, *Nature Reviews Microbiology 2004 2:2* **2004**, *2*, 95–108.
[14] W. Bokranz, X. Wang, H. Tschäpe, U. Römling, *J Med Microbiol* **2005**, *54*, 1171–1182.
[15] X. Zogaj, M. Nimtz, M. Rohde, W. Bokranz, U. Römling, *Mol Microbiol* **2001**, *39*, 1452–1463.
[16] W. Thongsomboon, D. O. Serra, A. Possling, C. Hadjineophytou, R. Hengge, L. Cegelski, *Science (1979)* **2018**, *359*, 334–338.
[17] D. O. Serra, A. M. Richter, G. Klauck, F. Mika, R. Hengge, *mBio* **2013**, *4*, 103–116.
[18] A. Olsén, A. Jonsson, S. Normark, *Nature 1989 338:6217* **1989**, *338*, 652–655.
[19] M. R. Chapman, L. S. Robinson, J. S. Pinkner, R. Roth, J. Heuser, M. Hammar, S. Normark, S. J. Hultgren, *Science* **2002**, *295*, 851–5.
[20] L. Cegelski, J. S. Pinkner, N. D. Hammer, C. K. Cusumano, C. S. Hung, E. Chorell, V. Åberg, J. N. Walker, P. C. Seed, F. Almqvist, M. R. Chapman, S. J. Hultgren, *Nat Chem Biol* **2009**, *5*, 913–919.
[21] C. Hung, J. Marschall, C. A. D. Burnham, A. S. Byun, J. P. Henderson, *PLoS One* **2014**, *9*, e86009.
[22] N. T. K. Nhu, M. D. Phan, K. M. Peters, A. W. Lo, B. M. Forde, T. M. Chong, W. F. Yin, K. G. Chan, M. Chromek, A. Brauner, M. R. Chapman, S. A. Beatson, M. A. Schembri, *mBio* **2018**, *9*, DOI 10.1128/MBIO.01462-18/SUPPL_FILE/MBO004184010SF3.TIF.
[23] E. C. Hollenbeck, A. Antonoplis, C. Chai, W. Thongsomboon, G. G. Fuller, L. Cegelski, *Proc Natl Acad Sci U S A* **2018**, *115*, 10106–10111.
[24] Z. Bian, A. Brauner, Y. Li, S. Normark, *Journal of Infectious Diseases* **2000**, *181*, 602–612.
[25] Ç. Tükel, J. H. Nishimori, R. P. Wilson, M. G. Winter, A. M. Keestra, J. P. M. Van Putten, A. J. Bäumler, *Cell Microbiol* **2010**, *12*, 1495–1505.
[26] G. J. Rapsinski, T. N. Newman, G. O. Oppong, J. P. M. Van Putten, C. Tüke, *Journal of Biological Chemistry* **2013**, *288*, 14178–14188.
[27] Y. Kai-Larsen, P. Lüthje, M. Chromek, V. Peters, X. Wang, A. Holm, L. Kádas, K.-O. Hedlund, J. Johansson, M. R. Chapman, S. H. Jacobson, U. Römling, B. Agerberth, A. Brauner, *PLoS Pathog* **2010**, *6*, e1001010.
[28] C. Wang, C. Y. Lau, F. Ma, C. Zheng, *Proc Natl Acad Sci U S A* **2021**, *118*, DOI 10.1073/PNAS.2106504118.
[29] T. R. Sampson, C. Challis, N. Jain, A. Moiseyenko, M. S. Ladinsky, G. G. Shastri, T. Thron, B. D. Needham, I. Horvath, J. W. Debelius, S. Janssen, R. Knight, P. Wittung-Stafshede, V. Gradinaru, M. Chapman, S. K. Mazmanian, *Elife* **2020**, *9*, DOI 10.7554/ELIFE.53111.
[30] S. G. Chen, V. Stribinskis, M. J. Rane, D. R. Demuth, E. Gozal, A. M. Roberts, R. Jagadapillai, R. Liu, K. Choe, B. Shivakumar, F. Son, S. Jin, R. Kerber, A. Adame, E. Masliah, R. P. Friedland, *Scientific Reports 2016 6:1* **2016**, *6*, 1–10.
[31] P. Wittung-Stafshede, *Curr Opin Struct Biol* **2022**, *72*, 33–38.
[32] A. L. Miller, S. Bessho, K. Grando, Ç. Tükel, *Front Immunol* **2021**, *12*, 514.
[33] X. Wang, M. Rochon, A. Lamprokostopoulou, H. Lünsdorf, M. Nimtz, U. Römling, *Cellular and Molecular Life Sciences* **2006**, *63*, 2352–2363.
[34] A. M. Richter, T. L. Povolotsky, L. H. Wieler, R. Hengge, *EMBO Mol Med* **2014**, *6*, 1622–1637.
[35] H. Karch, E. Denamur, U. Dobrindt, B. B. Finlay, R. Hengge, L. Johannes, E. Z. Ron, T. Tønjum, P. J. Sansonetti, M. Vicente, *EMBO Mol Med* **2012**, *4*, 841–848.
[36] L. S. Robinson, E. M. Ashman, S. J. Hultgren, M. R. Chapman, *Mol Microbiol* **2006**, *59*, 870–81.
[37] P. Goyal, P. V. Krasteva, N. Van Gerven, F. Gubellini, I. Van Den Broeck, A. Troupiotis-Tsaïlaki, W. Jonckheere, G. Péhau-Arnaudet, J. S. Pinkner, M. R. Chapman, S. J. Hultgren, S. Howorka, R. Fronzes, H. Remaut, *Nature 2014 516:7530* **2014**, *516*, 250–253.
[38] H. Loferer, M. Hammar, S. Normark, *Mol Microbiol* **1997**, *26*, 11–23.
[39] A. A. Nenninger, L. S. Robinson, S. J. Hultgren, *Proc Natl Acad Sci U S A* **2009**, *106*, 900–905.
[40] T. Schubeis, J. Spehr, J. Viereck, M. Nagaraj, M. Ahmed, C. Ritter, P. addressess, *Wiley Online Library* **2018**, *592*, 1020–1029.
[41] M. Hammar, A. Arnqvist, Z. Bian, A. Olsén, S. Normark, *Mol Microbiol* **1995**, *18*, 661–670.
[42] A. A. Nenninger, L. S. Robinson, N. D. Hammer, E. A. Epstein, M. P. Badtke, S. J. Hultgren, M. R. Chapman, *Mol Microbiol* **2011**, 1–14.
[43] R. D. Klein, Q. Shu, Z. T. Cusumano, K. Nagamatsu, N. C. Gualberto, A. J. L. Lynch, C. Wu, W. Wang, N. Jain, J. S. Pinkner, G. K. Amarasinghe, S. J. Hultgren, C. Frieden, M. R. Chapman, *mBio* **2018**, *9*, DOI 10.1128/mBio.01349-18.
[44] E. K. Andersson, C. Bengtsson, M. L. Evans, E. Chorell, M. Sellstedt, A. E. G. Lindgren, D. A. Hufnagel, M. Bhattacharya, P. M. Tessier, P.

Wittung-Stafshede, F. Almqvist, M. R. Chapman, *Chem Biol* **2013**, *20*, 1245–1254.
[45] D. Romero, E. Sanabria-Valentín, H. Vlamakis, R. Kolter, *Chem Biol* **2013**, *20*, 102–110.
[46] B. S. James McKechnie, Iain C. Paul, G. Schroeter, L. Lichtenstadt, D. Irineu, *J. Amer. C h e w SOC* **1918**, *51*, 22.
[47] K. Ono, L. Li, Y. Takamura, Y. Yoshiike, L. Zhu, F. Han, X. Mao, T. Ikeda, J. I. Takasaki, H. Nishijo, A. Takashima, D. B. Teplow, M. G. Zagorski, M. Yamada, *Journal of Biological Chemistry* **2012**, *287*, 14631–14643.
[48] M. Necula, R. Kayed, S. Milton, C. G. Glabe, *Journal of Biological Chemistry* **2007**, *282*, 10311–10324.
[49] M. Yamada, K. Ono, T. Hamaguchi, M. Noguchi-Shinohara, *Adv Exp Med Biol* **2015**, *863*, 79–95.
[50] M. J. Daniels, J. B. Nourse, H. Kim, V. Sainati, M. Schiavina, M. G. Murrali, B. Pan, J. J. Ferrie, C. M. Haney, R. Moons, N. S. Gould, A. Natalello, R. Grandori, F. Sobott, E. J. Petersson, E. Rhoades, R. Pierattelli, I. Felli, V. N. Uversky, K. A. Caldwell, G. A. Caldwell, E. S. Krol, H. Ischiropoulos, *Sci Rep* **2019**, *9*, 2937–2937.
[51] G. Bernardes, O. Munir, E. S. Krol, *Bioorg Med Chem* **2023**, *78*, 117147.
[52] Y. Porat, A. Abramowitz, E. Gazit, *Chem Biol Drug Des* **2006**, *67*, 27–37.
[53] C. Reichhardt, A. N. Jacobson, M. C. Maher, J. Uang, O. A. McCrate, M. Eckart, L. Cegelski, *PLoS One* **2015**, *10*, e0140388.
[54] C. Reichhardt, O. A. McCrate, X. Zhou, J. Lee, W. Thongsomboon, L. Cegelski, *Anal Bioanal Chem* **2016**, *408*, 7709–7717.
[55] S. K. Collinson, P. C. Doig, J. L. Doran, S. Clouthier, T. J. Trust, W. W. Kay, *J Bacteriol* **1993**, *175*, 12–18.
[56] S. Arteaga, A. Andrade-Cetto, R. Cárdenas, *J Ethnopharmacol* **2005**, *98*, 231–239.
[57] G. Manda, A. I. Rojo, E. Martínez-Klimova, J. Pedraza-Chaverri, A. Cuadrado, *Front Pharmacol* **2020**, *11*, 151.
[58] Y. Zhou, D. R. Smith, D. A. Hufnagel, M. R. Chapman, *Methods in Molecular Biology* **2013**, *966*, 53–75.
[59] M. M. Barnhart, M. R. Chapman, *Annu Rev Microbiol* **2006**, *60*, 131–47.
[60] M. L. Evans, M. R. Chapman, *Biochim Biophys Acta Mol Cell Res* **2014**, *1843*, 1551–1558.
[61] C. L. Patten, M. G. Kirchhof, M. R. Schertzberg, R. A. Morton, H. E. Schellhorn, *Molecular Genetics and Genomics* **2004**, *272*, 580–591.
[62] P. Sanchez-Vazquez, C. N. Dewey, N. Kitten, W. Ross, R. L. Gourse, *National Acad Sciences* **2019**, *116*, 8310–8319.
[63] R. C. Fink, E. P. Black, Z. Hou, M. Sugawara, M. J. Sadowsky, F. Diez-Gonzalez, *Appl Environ Microbiol* **2012**, *78*, 3783.
[64] J. S. Yuan, A. Reed, F. Chen, C. N. Stewart, *BMC Bioinformatics* **2006**, *7*, 1–12.
[65] J. Y. Lim, J. S. Pinkner, L. Cegelski, *Biochem Biophys Res Commun* **2014**, *443*, 345–350.
[66] E. K. Andersson, C. Bengtsson, M. L. Evans, E. Chorell, M. Sellstedt, A. E. G. Lindgren, D. A. Hufnagel, M. Bhattacharya, P. M. Tessier, P. Wittung-Stafshede, F. Almqvist, M. R. Chapman, *Chem Biol* **2013**, *20*, 1245–1254.
[67] P. I. Watnick, R. Kolter, *Mol Microbiol* **1999**, *34*, 586–595.
[68] P. I. Watnick, C. M. Lauriano, K. E. Klose, L. Croal, R. Kolter, *Mol Microbiol* **2001**, *39*, 223–235.
[69] G. A. O'Toole, R. Kolter, *Mol Microbiol* **1998**, *28*, 449–461.
[70] W. Herth, E. Schnepf, *Protoplasma* **1980**, *105*, 129–133.
[71] W. Thongsomboon, S. H. Werby, L. Cegelski, *J Bacteriol* **2020**, *202*, DOI 10.1128/JB.00030-20.
[72] M. C. Maher, J. Y. Lim, C. Gunawan, L. Cegelski, *ACS Infect Dis* **2016**, *1*, 460–468.
[73] J. D. Taylor, Y. Zhou, P. S. Salgado, A. Patwardhan, M. McGuffie, T. Pape, G. Grabe, E. Ashman, S. C. Constable, P. J. Simpson, and W. C. Lee, *Structure* **2011**,*19*,1307-1316.
[74] D. O. Serra, F. Mika, A. M. Richter, and R. Hengge, *Mol Microbiol* **2016**, *101*, 136-151.
[75] M. Pruteanu, J. I. Hernández Lobato, T. Stach, and R. Hengge, *Environ Microbiol* **2020**, *22*, 5280-5299.
[76] M. W. Pfaffl, *Nucleic Acids Res* **2001**, *29*, e45–e45.

Entry for the Table of Contents

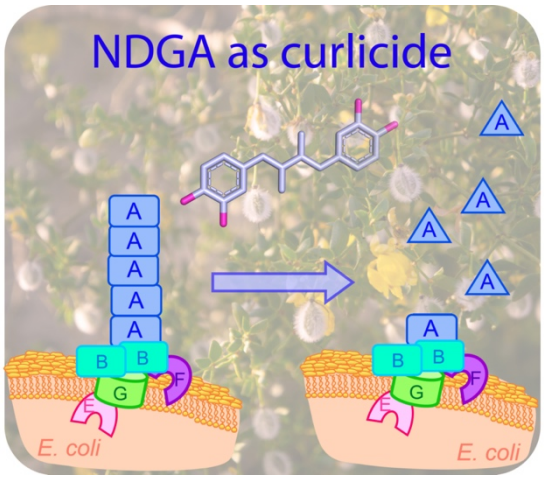

The natural product nordihydroguaiaretic acid (NDGA) found in the creosote bush is a curlicide. NDGA inhibits *in vitro* polymerization of the bacterial amyloid protein CsgA and inhibits cellular amyloid biogenesis in *E. coli*. NDGA's curlicide activity is effective in inhibiting biofilm formation by pathogenic *E. coli* and *Salmonella* Typhimurium.

SUPPORTING INFORMATION

Nordihydroguaiaretic Acid (NDGA) Inhibits CsgA Polymerization, Bacterial Amyloid Biogenesis, and Biofilm Formation

Joshua A. Visser,[1] Deborah Yager,[1] Schuyler A. Chambers,[1] Ji Youn Lim,[1] Xujun Cao,[1] and Lynette Cegelski[1]*

[1]Department of Chemistry, 380 Roth Way, Stanford University, Stanford, California 94305

[*]Corresponding author: cegelski@stanford.edu

Table of Contents

SUPPORTING FIGURES

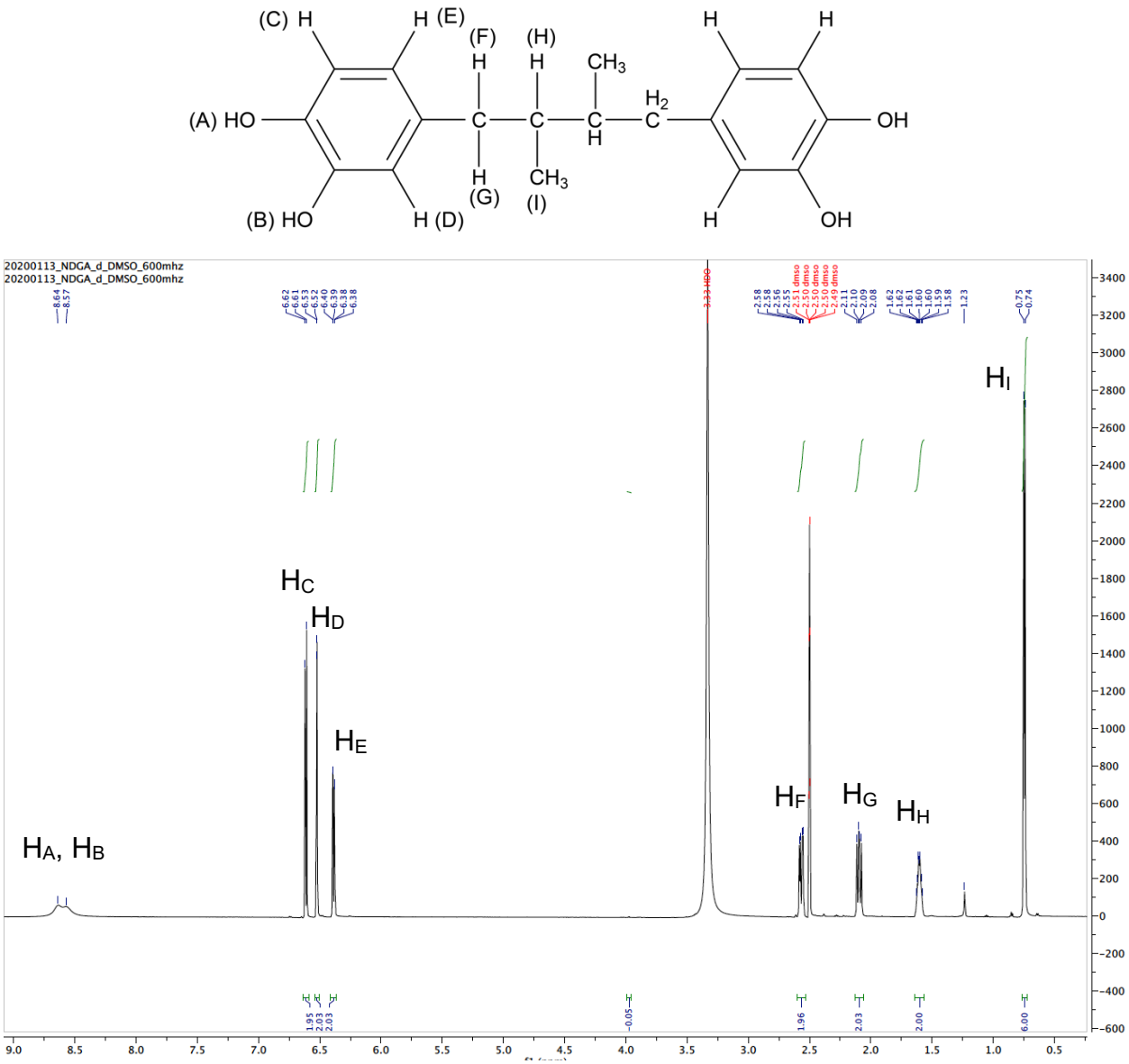

Figure S1. Solution NMR spectrum of NDGA. 1H NMR (d6-DMSO, 600 MHz): δ= 8.64 (b, 1H, HA), 8.57 (b, 1H, HB), 6.61 (d, 2H, HC), 6.52 (d, 2H, HD), 6.39 (dd, 2H, HE), 2.57 (dd, 2H, HF), 2.10 (dd, 2H, HG), 1.60 (m, 2H, HH), 0.74 (d, 6H, HI). Chemical shift values agree with expected values. Integration of all C-H bonds align with expected values. Aromatic-OH integration is lower than expected due to rapid exchange with water. Peaks at 3.33 and 2.5 correspond to water and DMSO, respectively.

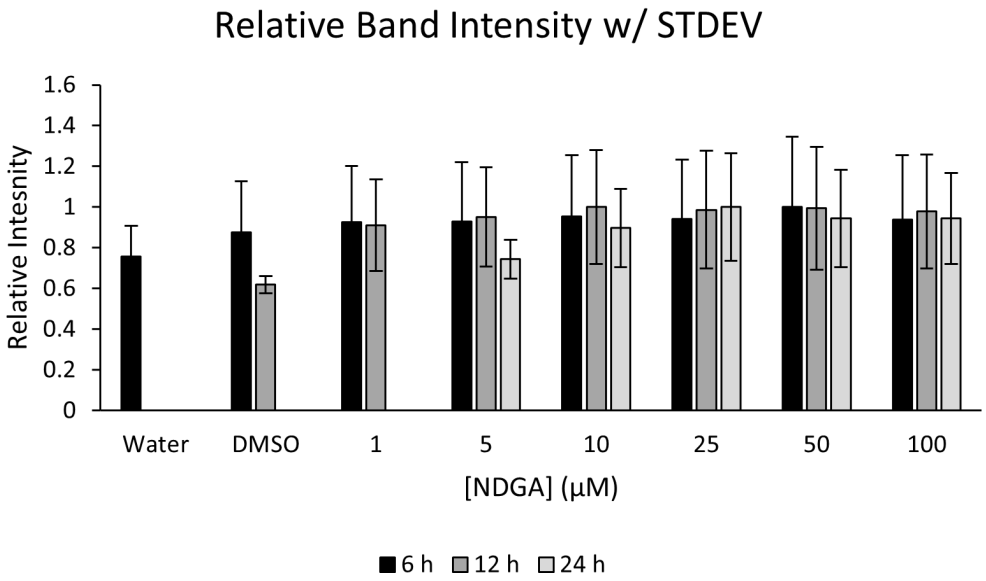

Figure S2. Relative band intensities through densitometry analysis of His_6-CsgA bands in the SDS-PAGE gel in Figure 1B. The averages of the grayscale values (mean gray value) within each square region of interest are plotted +/- standard deviation corresponding to the density values of pixels for the given bands. Standard deviation within the selection represents the deviation of grayscale value within the square.

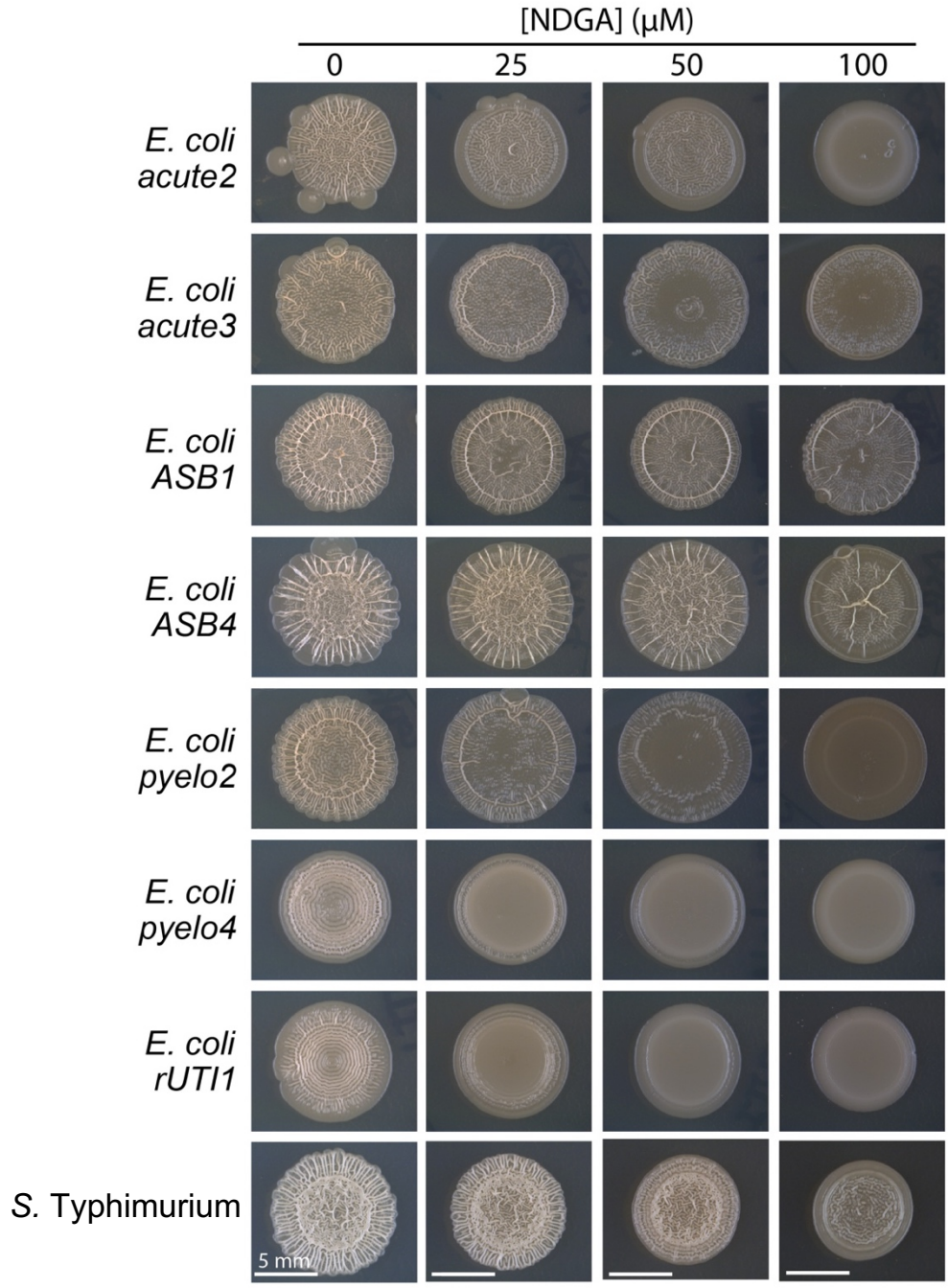

Figure S3. NDGA inhibits macrocolony architecture of uropathogenic *E. coli* clinical isolates and *Salmonella enterica* serotype Typhimurium (*S.* Typhimurium). Macrocolonies resulted from the growth of bacteria from liquid drop cultures of each strain grown on YESCA agar supplemented with specified concentrations of NDGA, each associated with a final DMSO concentration of 0.4% vol/vol. NDGA inhibited the wrinkling phenotype in all strains.

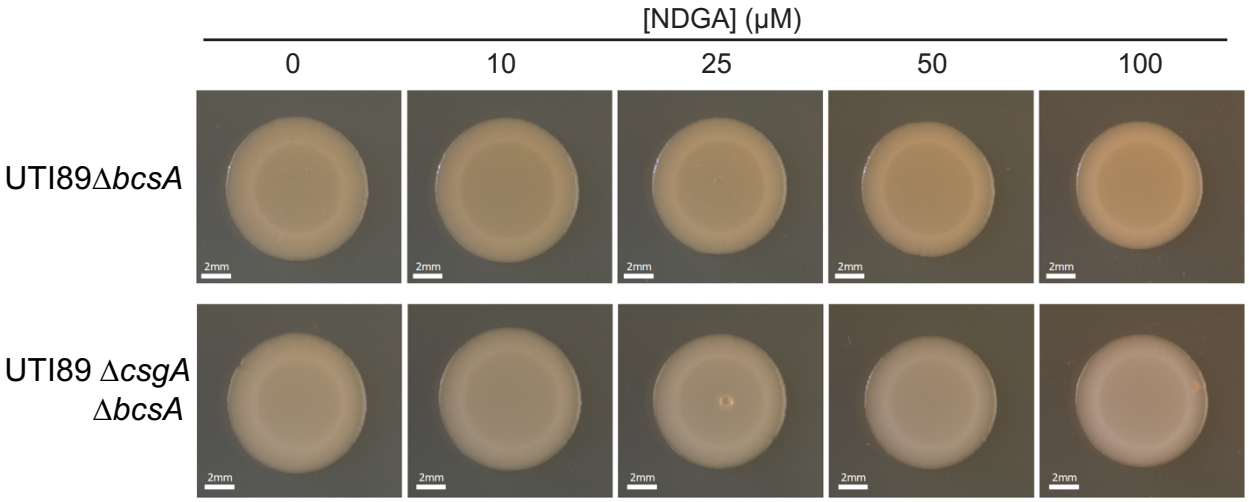

Figure S4. Macrocolony architecture of UTI89 mutants grown from liquid drop cultures on YESCA agar supplemented with specified concentrations of NDGA, each associated with a final DMSO concentration of 0.4% vol/vol. NDGA does not influence the smooth microcolony morphology of UTI89Δ*bcsA or* UTI89Δ*csgA*Δ*bcsA*.

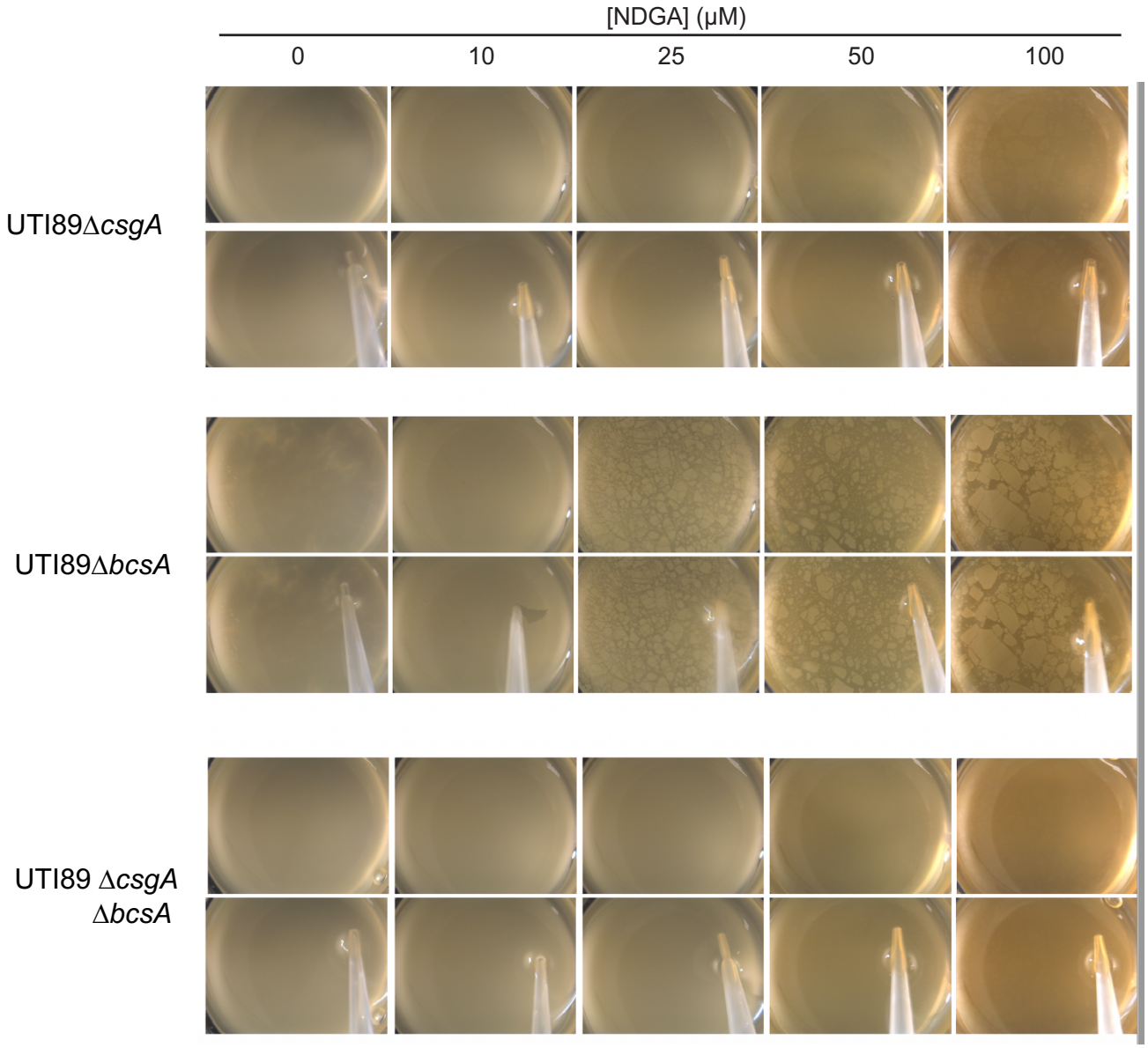

Figure S5. Pellicle architecture of UTI89 mutants grown in YESCA broth supplemented with specified concentrations of NDGA, each associated with a final DMSO concentration of 0.4% vol/vol. NDGA exhibits inhibition of the delicate curli-associated pellicle that is formed by UTI89Δ*bcsA*. UTI89Δ*csgA* and UTI89Δ*csgA* Δ*bcsA* do not form appreciable pellicles and this is unchanged with NDGA treatment.

Supporting Experimental Procedures

Quantification and Densitometry of His_6-CsgA bands in SDS-PAGE gel.

The protein gel bands from Figure 1B were analyzed using ImageJ (NIH), a public domain program from the National Institutes of Health. Densitometry analysis is provided in Figure S1. Images from the gel were imported into ImageJ with the default image size and converted into 8-bit images. ImageJ's threshold pixel values were set to a minimum of 115 arbitrary units (au) and maximum of 212 au to encapsulate all bands in the image without oversaturation. The adjustment was made using the histogram of the image, wherein for each 8-bit image, the histogram represents the results of 256 bins over the range of grayscale values of the selected image. Due to the set threshold values, background subtraction was not included as the background had a density value below that of the minimum set during thresholding. A square region of interest was created to encapsulate each band, positioned at the center of the band. The profiles of the bands are represented as the average of the grayscale values (mean gray value) within the square region of interest. Standard deviation within the selection represents the deviation of grayscale value within the square. Relative band intensities were computed using the highest band intensity from each time point as the standard.